Langevin dynamic predictions of polymer-particle adsorption and saturation in shear flows

L.F. Mortimer [*], M. Fairweather

School of Chemical and Process Engineering, University of Leeds, Leeds LS2 9JT, UK

ABSTRACT

Polymer-particle interactions, adsorption and subsequent polymer saturation in shear flows are studied using Langevin dynamics and a potential-based interaction modelling technique in a three-dimensional domain containing a single fixed particle. The polymeric phase is modelled as macromolecular chains of interacting beads (monomers), with the effects of bead-bead and bead-particle steric interactions incorporated through a truncated Lennard-Jones potential. To further account for polymer flexibility, the Kratky-Porod bending rigidity is also accounted for. Simulation ensembles of 100 multi-polymer particle adsorption events within a pre-obtained shear flow are performed for each parameter set studied, with the effects of bending rigidity, FENE potential strength and polymer concentration examined. It is found that for low bending rigidities, polymers are more likely to fully adsorb onto the particle, with conformities tightly bound and flattened to the spherical surface. Increased rigidities cause polymer chains to hang away from the particle surface. Around 75% adsorption is achieved for low rigidity polymers whereas for high rigidity, just over half of the monomers tend to remain bound. Furthermore, it is demonstrated that increasing the rigidity leads to more monomers present in the surrounding area adsorption zone, constituting an increase in effective radius. Results indicate that the FENE potential strength also significantly impacts adsorption kinetics, with lower interaction strengths favouring increased adsorption efficiency and longer tails, ideal for flocculation purposes. Conversely, increased FENE interaction strengths lead to reduced full adsorption probability and shorter tails. Finally, the influence of initial polymer concentration on adsorption behaviour and surface saturation is investigated. Higher concentrations result in decreased adsorption efficiency and increased surface monomer saturation, affecting polymer conformations and interaction dynamics such that the potential for important processes such as bridging is hindered. These findings offer valuable insights for optimising polymer adsorption processes in practical applications such as flocculation and settling.

1. Introduction

Optimized filtration and thickening stands as an industrial challenge across many applications, such as water treatment, chemical manufacture and nuclear waste processing (Lockwood et al., 2021). Various techniques are in development to aid these processes. For instance, low concentrations of high molecular weight polymers are often added to aqueous particle-laden suspensions in order to separate the non-settling solid phase. In recent decades, there has been significant research focus on the use of polymeric settling agents (Heath et al., 2006; Zhou and Franks, 2006). This method has proven effective in enhancing processes such as filtration and thickening across various industrial domains (Lockwood et al., 2021; Vajihinejad et al., 2019; Lee et al., 2014).

Particularly relevant to the present study is its application in nuclear decommissioning settings, where it offers benefits such as reducing turbidity and enhancing settling and sediment consolidation rates (Joseph-Soly et al., 2019). Moreover, polymeric flocculants find utility beyond industrial contexts. The concern over the immobilization and elimination of trace metal elements and pesticides from rivers, arising from natural and industrial sources, is escalating. Both organic and inorganic contaminant molecules are transported, necessitating the aggregation of polymeric colloidal particles (with diameters below 1 μm) to enable settling in such flows. Occasionally, a phenomenon occurs where microorganisms release fibrillar extracellular polymeric substances into river or water ecosystems, naturally facilitating flocculation (Buffle and Leppard, 1995; Stoll and Buffle, 1996).

Though having demonstrated their efficacy in laboratory scale rigs, polymer additives and their particle adsorption dynamics are complex to predict and so optimisation of these systems is difficult with present knowledge (Dickinson and Eriksson, 1991). Usually, the advantageous attributes of both natural and synthetic polymers are utilized to customize their characteristics for optimal particle adsorption efficiency (Vajihinejad et al., 2019), a process known as behavioural modification. Lacking a comprehensive understanding of how polymer properties influence subsequent adsorption and flocculation results in poor predictability of optimal system parameters for desired outcomes, leading to inefficient implementation of these techniques. The solid phase particle diameter range tends to span across nano- to micro-scales and flocculation is therefore used to increase the mean cluster size in order to improve the ease of removal. Furthermore, to use polymer flocculation in sensitive systems such as nuclear waste settling tanks and flows, the effectiveness and resultant behaviour must be fully proven, demonstrated and understood. One key challenge lies in predicting the process of steric stabilization, which occurs at high adsorption densities, wherein adsorbed nonionic polymers inhibit further flocculation by producing a strong repulsion between the particles. This reduces the effectiveness of bridging, wherein polymers span the gap between nearby particles (leading to flocculation) by shielding available adsorption sites on the particle surface. The polymer itself inherently possesses properties such as the bond angle between monomers which influences torsional potentials. These properties' overall impact on polymer conformity is often described by a parameter known as the 'persistence length' (Khokhlov et al., 1994), which quantifies bending stiffness. Experimental evidence suggests that ionic strength also influences the persistence length, with higher ionic strengths leading to charge screening and the adoption of more coil-like conformations with lower persistence lengths (Colby, 2010). The Kratky-Porod model is frequently employed to describe semi-flexible polymers, which postulates that the energetic cost of bending is quadratically related to the bending angle (Vologodskii and Frank-Kamenetskii, 2013). Various approaches have been proposed within this model to estimate the effective persistence length (Popov and Tkachenko, 2005; Kulić et al., 2005). Increased bending rigidity restricts polymer chain flexibility, impeding their ability to conform around particles and bridge effectively. Consequently, this also influences a polymer's capability to establish robust connections between particles, thereby impacting the strength and stability of resultant flocculants (Mortimer and Fairweather, 2023). The fundamental dynamics of interactions between polymers and particles is also of interest in the polymer synthesis industry, where studies have demonstrated that nanoparticles can impact various characteristics of polymer nanocomposites, including viscosity (Mackay et al., 2003), glass transition temperature (Starr et al., 2001), and electrical conductivity (White et al., 2010).

The application of polymer-phase modelling (Öttinger, 2012) has been used in recent years, uncovering various interesting phenomena for simple interacting systems in both stagnant environments (Smith et al., 1999), as well as shear or turbulent flows (Fu and Kawaguchi, 2013). Previous studies considering single polymer-particle interaction events demonstrated that bending rigidity plays an important role in the final structure upon adsorption, with increased bending rigidities leading to longer tails (Mortimer and Fairweather, 2023), promoting the bridging mechanism. Monte-Carlo and Metropolis modelling has shown that the conformities formed by the interaction between polymers and particles rely heavily on the strength of the interaction potentials (Li et al., 2016). When the interaction strength is higher, the proportion of trains to tails and loops in the resulting structure tends to increase. Experimental evidence has also demonstrated that polymers within shear flows exhibit elongational and rotational mechanisms, resulting in tumbling motions. This phenomenon adds complexity to the behaviour of polymer-particle interactions (He et al., 2009; He et al., 2010). Studies have also revealed that the final flocculant structure is influenced by the properties of the polymer. For instance, porous flocculated structures can be disrupted by

fluid shear, indicating their sensitivity to external forces (Tambo, 1991).

In this study, we aim to determine the extent to which key parameters such as bending rigidity and finitely extensible nonlinear elastic (FENE) potential strength are capable of encouraging the bridging mechanism in the steric stabilization regime. Natural flocculants can be combined with synthetic polymers tailored to ideal conditions, improving the efficiency of the flocculation processes. With knowledge surrounding the flocculation dynamics on the particle scale, these optimizations can be improved. Here, nonequilibrium Langevin dynamics is used to predict polymer-particle interaction and adsorption in shear flow conditions, as applied in various other studies (Li et al., 2016; Brackley et al., 2020; Mortimer et al., 2023). We explore the methods by which adsorption saturation and steric stabilization occurs and determine how the polymeric phase parameters can offer various conformities as the adsorption density increases. The advancement of the current technique also establishes a basis for investigating rheological flows by examining the interaction between polymer conformation and the fluid stress tensor at a local level. This framework also enables the exploration of processes such as drag reduction and viscoelasticity, facilitating further research in this field.

2. Methodology

The present work uses Langevin dynamics as well as the FENE polymer model to predict the motion of polymer chains in a pre-obtained steady shear flow in the presence of a fixed spherical particle. In typical shear and turbulent flows, particle diameters are often sub-Kolmogorov, which provides confidence in the assumption that the shear rate is constant across the surface of the particle and within its local fluid region. This means that by fixing the particle in the centre of the domain, we are considering the reference frame of the particle which is interacting with multiple polymer chains in a region of local shear.

The polymer dynamics described below have been employed in various Brownian dynamic studies (Doyle et al., 1998; Li et al., 2017; Brackley, 2020), though prediction of adsorption is very rare in the literature, with no studies performing Monte-Carlo based analysis in shear flows to the authors' knowledge. Polymers themselves are represented as macromolecular chains of interacting monomer beads, as illustrated in Fig. 1, with each bead's trajectory calculated using the Newtonian equation of motion (Öttinger, 2012):

$$m_b \frac{d^2 \boldsymbol{r}_i}{dt^2} = -\nabla V_i - \xi \left(\frac{d\boldsymbol{r}_i}{dt} - \boldsymbol{u}_{F,i} \right) + \sqrt{2k_B T \xi} \boldsymbol{\eta}_i(t). \tag{1}$$

Here, $\boldsymbol{r}_i$ is the position vector of bead i in the chain, m_b is the mass of
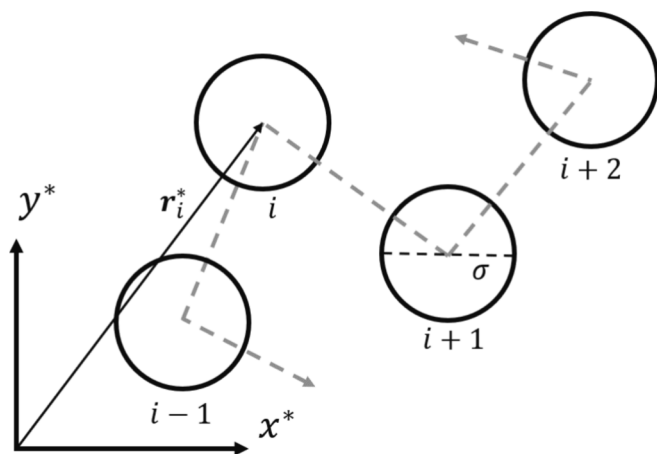

Fig. 1. Schematic of a single modelled monomer chain forming a polymer. Dashed lines represent fictional springs connecting monomer beads (solid circles).

the bead, ξ is the drag coefficient, $\boldsymbol{u}_{F,i}$ is the fluid velocity obtained from the simulated shear flow steady state and interpolated at the bead position, k_B is Boltzmann's constant and $\boldsymbol{\eta}_i(t)$ is a Brownian noise term which satisfies $\langle \eta_{ia}(t) \rangle = 0$ and $\langle \eta_{ia}(t)\eta_{ib}(t') \rangle = \delta_{a,b}\delta(t-t')$. This equation is solved in non-dimensional form, with the space timescale using the bead diameter, σ, and time using the Brownian bead timescale, $\tau_b = \sqrt{m_b\sigma/k_BT}$. Introducing the diffusion coefficient, $D = k_BT/\xi$, we may rewrite Eq. (1) in non-dimensional form as:

$$\frac{d^2 r_i^*}{dt^{*2}} = -\nabla V_i^* - \frac{1}{D}\left(\frac{dr_i^*}{dt^*} - u_{F,i}^*\right) + \sqrt{\frac{2}{D}}\eta_i^*(t^*). \tag{2}$$

In this equation, variables denoted with (*) indicate non-dimensional terms. The individual contributions to the overall interaction potential for the beads are provided as follows:

$$V_i^* = V_{i,F}^* + V_{i,B}^* + V_{i,W}^* + V_{i,P}^*. \tag{3}$$

The term $V_{i,F}^*$ represents the bonding between the monomers using the finitely extensible nonlinear elastic spring force potential. This force is described by:

$$V_{i,F}^*(\delta r^*) = -\frac{K_F^* R_0^{*2}}{2}\ln\left[1 - \left(\frac{\delta r^*}{R_0^*}\right)^2\right]. \tag{4}$$

Here, $\delta r^* = |r_{i+1}^* - r_i^*|$ represents the separation between beads, $K_F^* = K_F/k_BT$ is the energy scale of the FENE potential, and R_0^* is the maximum FENE bond length. This interaction potential is considered only for adjacent beads within the polymer chain. The second term accounts for the impact of polymer bending rigidity observed in actual polymers, where energetically unfavourable acute polymer angles arise due to molecular constraints. The Kratky-Porod potential is expressed as:

$$V_{i,B}^*(\theta_i) = K_B^*(1 + \cos(\theta_i)), \tag{5}$$

where θ_i is the angle formed by two neighbouring bead separation vectors, i.e. $\theta_i = \cos^{-1}(\hat{\boldsymbol{n}}_{i+1}\cdot\hat{\boldsymbol{n}}_i)$ with $\hat{\boldsymbol{n}}_i = (r_i^* - r_{i+1}^*)/|r_i^* - r_{i+1}^*|$. The bending rigidity strength is denoted by K_B^*. The second to last term in Eq. (3) accounts for steric interactions among polymer beads and is described by a Weeks-Chandler-Anderson potential:

$$V_{i,W}^*(\delta r^*) = 1 + 4\left[\left(\frac{\sigma}{\delta r^*}\right)^{12} - \left(\frac{\sigma}{\delta r^*}\right)^6\right]. \tag{6}$$

This term adds to the overall potential between pairs of monomers within a maximum distance δr_{max}^*, accounting for their inability to occupy the same spatial location. The last term in Eq. (3) accounts for the interaction with a dispersed particulate phase. The particles are represented as isotropic spheres of constant diameter, $D_P = 10\sigma$. In all simulations considered in this context, the particle remains fixed at the centre of the computational domain. Polymer beads in proximity to the particle experience steric interactions. The interaction potential between the polymer and particle is a truncated Lennard-Jones potential, given by (Li et al., 2017):

$$V_{i,P}^*(\delta r^*) = K_{LJT}^*\left[\left(\frac{1}{\delta r^* - s^*}\right)^{12} - 2\left(\frac{1}{\delta r^* - s^*}\right)^6\right] + V_{0,P}^*, \tag{7}$$

with the term $V_{0,P}^*$ representing a shift in the interaction potential such that $V_{i,P}^*(\delta r^* > 5) = 0$, given as:

$$V_{0,P}^*(\delta r^*) = K_{LJT}^*\left[\left(\frac{1}{2.5}\right)^{12} - 2\left(\frac{1}{2.5}\right)^6\right]. \tag{8}$$

The equations above are solved for each monomer bead using a Verlet-velocity integration scheme and constant timestep $\delta t^* = 0.005$. To study multi-polymer adsorption onto a stationary particle within a flow, the domain is a $60 \times 30 \times 30$ computational channel cell in all cases, with domain lengths presented in non-dimensional units using the bead length scale, σ. Periodic conditions are enforced in the streamwise (x^*) and spanwise (z^*) directions, while the wall-normal (y^*) direction extents use a wall potential, $V_{i,W}^*(\delta y^*) = 10\delta y^{*2}$, for wall penetration depth δy^*. The velocity of the lower wall is kept constant, $u_x^* = 0$, while the top wall moves with velocity $u_x^* = L_y^* We$, with L_y^* the vertical length and $We = 0.3$ the Weissenberg number. The steady state flow field was captured using the spectral element method-based direct numerical simulation solver, Nek5000 (Fischer et al., 2008) on a Cartesian mesh containing 54,000 elements. No-slip boundary conditions were enforced on the spherical surface at the centre of the domain, as well as upon the upper and lower walls ($y^* = -15, 15$), with the lower wall enforcing $u_x^* = 0$. 0 and the upper wall enforcing a standard Dirichlet velocity condition ($u_x^* = L_y^* We$). The Navier-Stokes equations were solved in non-dimensional form using the above non-dimensionalisation, using a constant timestep $dt_{DNS}^* = 1 \times 10^{-5}$ for $N_{T,DNS} = 50,000$ timesteps, with the final steady-state flow field used in the subsequent polymer-particle simulations, as illustrated in Fig. 2.

Upon obtaining this, and before the first polymer-particle simulation timestep, N_P polymer chains consisting of $N_{BPP} = 32$ connected beads are injected into the upstream region $x^* < 20$, with the particle of diameter $D_P^* = 10$ fixed stationary at $x^* = 30$. Mean behaviour dependence on the initial distribution and initial conformity of the polymer chains will hence be eliminated due to the nature of the Monte Carlo sampling method employed, and the high number of samples (100) used for all probability density functions presented within this study. The computational domain at injection of one realisation for the polymeric phase is illustrated in Fig. 3.

The properties used in all simulations considered here are presented in Table 1. Parameters listed in bold are used when other parameters are varied. Three important properties, the bending rigidity potential strength, K_B^*, the FENE potential strength, K_F^*, and the number of injected polymers (or polymer concentration), N_P, are studied in order to determine their influence on the conformation and structures formed during ensembles of simulated polymer-particle interaction events. Specific values, as well as the ranges of interaction strengths, were chosen to encompass those considered in previous studies in order to provide comparisons to such, as well as to expand understanding (Lang et al., 2014; Li et al., 2016; Li et al., 2017; Brackley, 2020).

3. Results and discussion

The interaction between flexible polymer chains and particle surfaces plays a crucial role in their subsequent flocculation dynamics in multiphase systems. In this analysis, the intricate dynamics of polymer adsorption onto surfaces are analysed, elucidated, and discussed through studying three dimensional Langevin dynamics simulations of the adsorption process instigated through advection within a shear flow in the presence of a single particle. Through simulations and statistical analyses, we investigate how variations in the bending rigidity potential strength, FENE potential strength and concentration impact the adsorption efficiency, polymer conformations, saturation and the formation of tails on the surface. Adopting a Monte-Carlo approach to study resulting conformities, simulation results presented here are averaged across 100 independent realisations of the shear flow, chosen to be a sufficient number in order to produce smooth probability distribution functions and negligible statistical error in temporal observations of final conformation properties. This number was decided on by comparing the results of one parameter set using 50, 100 and 150 realisations, with statistical noise observed in the former, and diminishing returns on sample number independence noted in the latter.

The Kratky-Porod bending rigidity potential, given by $V_{i,B}^*(\theta_i) = K_B^*(1 + \cos(\theta_i))$, has been demonstrated to influence the conformity of the polymer chain when adsorption takes place (Mortimer and
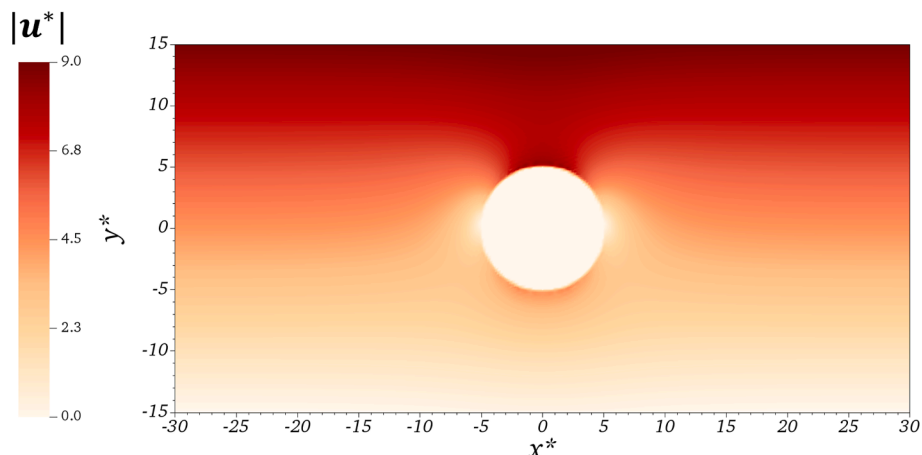
Fig. 2. Instantaneous pseudocolor plot of velocity magnitude representing the computational fluid flow field in the (x^*, y^*) plane through the midpoint of the shear channel containing a fixed spherical particle at the centre.
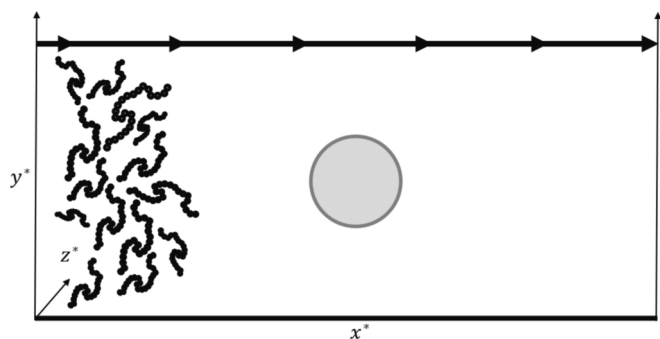

Fig. 3. Schematic illustrating the injection condition for an instance of multi polymer-particle adsorption interaction events.

Table 1
Polymer-particle adsorption simulation parameters. Parameters indicated in bold represent fixed 'base case' conditions when other parameters are varied.

Parameter	Value
R_0^*	1.6
We	0.3
D	5.0
D_P^*	10.0
K_F^*	10.0, **30.0**, 50.0
K_B^*	**1.0**, 3.0, 5.0
δt^*	0.005
N_P	**15**, 25, 35
N_{BPP}	32

Fairweather, 2023). Here, we consider the effect of the strength of this potential, which acts to restrict the bead chains from adopting acute angles, within shear flows. Fig. 4 illustrates the result of such interactions while varying the potential strength, K_B^*. At low bending rigidity, the result is that polymers are able to adsorb onto the particle with ease, flattening and spreading out across its surface. From the instantaneous snapshot from a single simulation in the ensemble, we observe that the surface coverage is high, with only a few loops and tails formed travelling away from the particle. As the rigidity is increased, the inability to flatten out onto the particle leads to more cluster-like polymer conformities forming on the particle, and longer structures leading to longer tails. These also tend to form parallel to the streamwise direction. Similar results are observed for $K_B^* = 5.0$ with most structures tending to be more train like, encircling the particle diameter in some

cases. To quantify the adsorption events, we consider a monomer to have adsorbed onto the particle if its distance from the particle surface is less than the monomer bead diameter ($dr^* < 1$).

In Fig. 5, the left plot compares the percentage of adsorbed monomers over time to ensure the length of each simulation in the ensemble chosen is suitable to capture the adsorption process. In each case, the percentage of adsorbed monomers, $N_A (\%)$, stabilises by the end of the simulation indicating that the adsorption process takes place by around $t^* = 10$. It is observed that for low bending rigidity, more monomers are capable of adsorbing onto the particle surface by the end of the interaction event. As the potential is increased, the longer conformities present means that full adsorption onto the surface is less energetically favourable, and so the percentage is reduced. The right plot in Fig. 5 tracks the percentage of monomers within the adsorption region, $N_R (\%)$, defined as ($1 \le dr^* \le d_P^*$), which would indicate the presence of tails. The maximum bead density within that region occurs for the low bending rigidity monomers but very rapidly decays indicating the full adsorption taking place over a short timeframe, and tails diminishing. The end result indicates that the polymers with $K_B^* = 3$ possess the largest tails, with around a third of their chains still present in the adsorption region, leading to a larger effective particle radius.

Results sampled from 100 Monte Carlo events for each bending rigidity potential strength considered are presented in Fig. 6, which considers the adsorption dynamics of each polymer in the system separately. The left plot illustrates the probability density functions of the number of adsorbed beads from each polymer. This analysis technique was chosen to fully capture the range of eventual conformities present for each parameter set, including the existence of rare events which could play an important role in bulk-scale dynamics, such as the infrequent existence of polymer tails which could subsequently form bridges with other particles. The distribution is bimodal in each case studied, with the left peak both representing polymers which did not remain bound to the particle after adsorption ($N_A = 0$), as well as rare events where tails are only around $1 - 6$ of the monomers adsorb, inducating the existence of tails or loops. For the two highest bending rigidity strengths, $K_B^* = 3.0$ and 5.0, polymers are less likely to either miss the particle or be removed from the surface, indicated by the less pronounced initial maximum. Since these polymers tend to have increased radii of gyration due to their tendency to straighten out more than the curled up $K_B^* = 1.0$ polymers, collision with the particle is more likely. We observe the greatest monomer adsorption for $K_B^* = 3.0$, with lower bending rigidities likely spreading out across the particle surface reducing vacancies for other polymer chains, and higher bending rigidities more likely to hang away from the particle as observed in single-polymer adsorption studies (Mortimer and Fairweather, 2023). Sintes
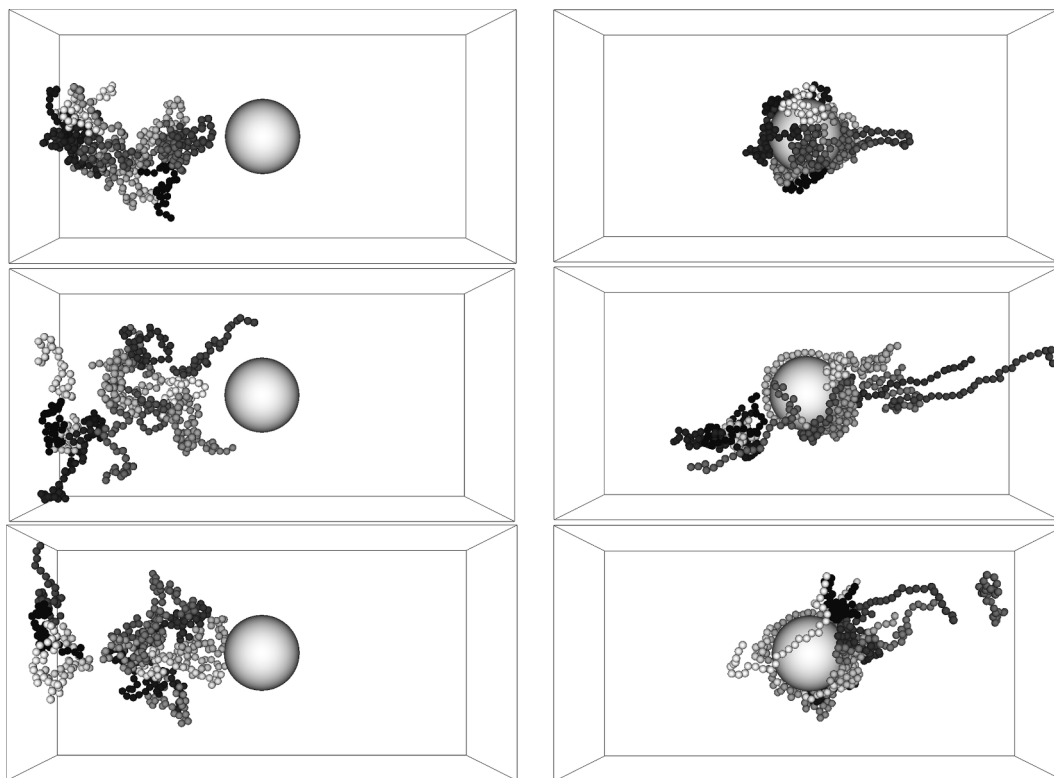
Fig. 4. Instantaneous snapshots of polymer-particle interaction at $t^* = 1$ (left) and $t^* = 10$ (right). Upper: $K_B^* = 1$; middle: $K_B^* = 3$; lower: $K_B^* = 5$.
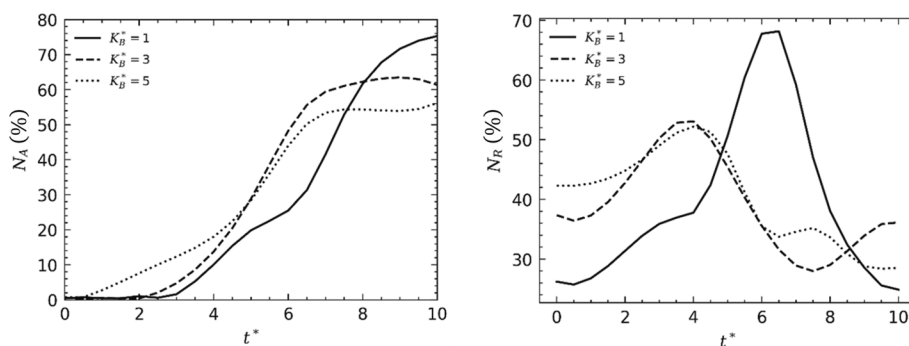

Fig. 5. Effect of bending rigidity potential strength on the temporal evolution of percentage of adsorbed monomers (left) and monomers in adsorption region $(1 \leq dr^* \leq d_P^*)$ (right).
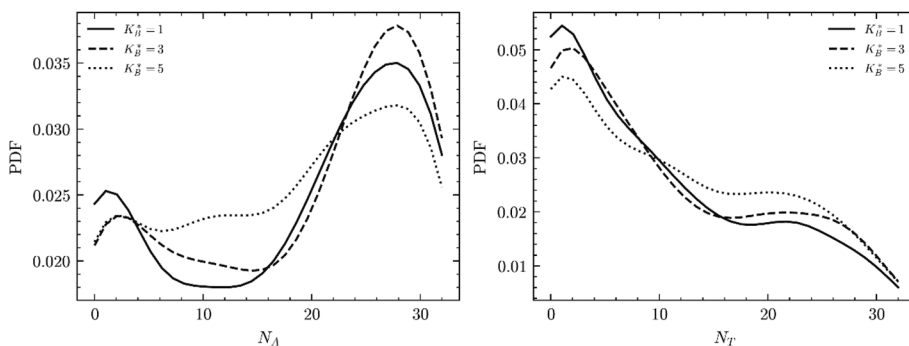

Fig. 6. Effect of bending rigidity potential strength on the probability density functions of the number of adsorbed beads from a single polymer, N_A (left), and number of tail beads, N_T (right).

et al. (2001) also observed increase adsorption onto flat surfaces as the stiffness of the polymer chain initially increased in off-lattice Monte Carlo simulation, though this effect persisted further into more rigid polymers, unlike the results observed here. This is likely because flat surfaces offer easier adsorption potential for a particular conformity, whereas on a curved surface, the more stretched out, rigid chains need to further bend, which is more energetically unfavourable as the bending rigidity potential strength increases. The right plot in Fig. 6 illustrates the number of tail beads present in attached polymers by the end of the simulation. Tail beads are counted as being connected to a polymer which has another monomer bead fully adsorbed onto the particle surface. For the purpose of this analysis, polymers which did not adsorb onto the particle at all are counted as possessing zero tail beads. As the bending rigidity is increased, the distribution increases its skew towards chains containing a greater amount of tail beads, in line with previous studies (Mortimer and Fairweather, 2023). Due to steric stabilization effects, the consideration of other polymers which have already adsorbed onto the surface leads to more tail beads present in the final structure when compared to single-polymer Monte Carlo studies. In a practical application, to instigate flocculation both adsorbed beads and tail beads must be present in order to avoid saturation of the particle surface before the effective interaction radius of the flocculant grows due to tails. High bending rigidities are hence shown to exhibit these properties, and chain stiffness has been demonstrated to possess the ability to be tuned by modifying the ionic strength of the carrier phase (Tree et al., 2013).

To further determine the extent of saturation of monomer adsorption leading to steric stabilization, the eventual state is now treated as a collection of individual monomer beads. Statistics were collected surrounding the positions of these beads in the final adsorbed state across all fifteen polymers, and 100 Monte Carlo samples were again used to generate the results.

Fig. 7 shows the effect of the bending rigidity on the percentage of the total number of beads which have been fully adsorbed. No simulations lead to zero monomers adsorbed, with at least 20% of the total beads adsorbing onto the particle surface in all cases. The $K_B^* = 1.0$ case has the lowest percentage peak, with around 30% of the total monomers reaching the particle, though interestingly, at this low bending rigidity, another peak occurs around 45%. Single-polymer studies (Mortimer and Fairweather, 2023) indicated that these spread out across the particle surface, reducing the area which further polymers can adsorb to due to their exclusion radii. Aside from this lowest chain stiffness which demonstrates a range of behaviour, as the bending rigidity increases, the modal percentage of beads which are fully adsorbed also increases.
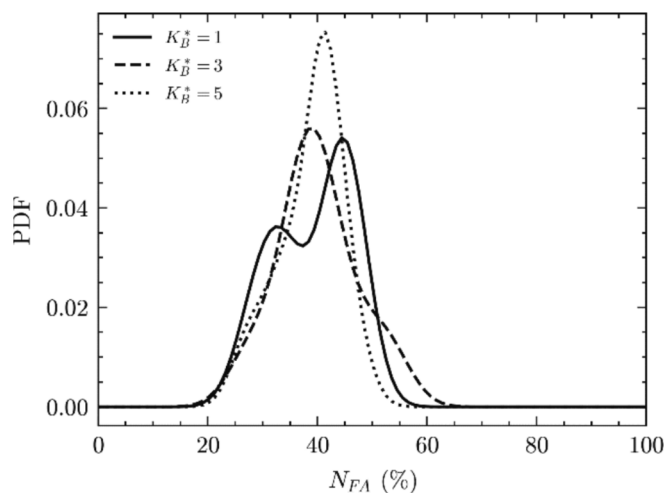
However, the largest adsorption percentage (around 60%) occurs at the midrange bending rigidity ($K_B^* = 3.0$). This is likely due to the medium rigidity polymer chains being capable of wrapping around the particle surface, rather than spreading out across a local region, leading to further, wider adsorption-capable areas.

Another important property of importance to adsorption dynamics is the strength of the FENE potential, K_F^*, which determines the mean separation distance between monomers in the polymer chain. Our previous work (Mortimer et al., 2023) demonstrated that lower FENE potential strengths lead to higher adsorption efficiency for a semi-adsorbed final state, wherein it is more likely to observe tails similar in length to the fully-adsorbed section of the polymer. This is ideal for practical flocculation purposes since the polymer remains tightly bound to the particle while still increasing its effective radius of gyration. Examples of final states for the FENE potential strength variation study are presented in Fig. 8. For the low K_F^*, the majority of polymers spread out across the particle surface with evidence of tails hanging away from the particle particularly in the streamwise direction in the region of increased fluid velocity. As the strength of the potential increases, we observe that full adsorption becomes less likely, with many polymers conforming around the particle, straightening out, with more polymers not fully adsorbing to the surface. Finally, at $K_F^* = 50$, we once again observe more adsorption, with larger tails when compared to the $K_F^* = 10$ simulation.

Probability density functions of the number of adsorbed beads and the number of tail beads are presented in Fig. 9. The highest likelihood of full adsorption of monomers onto the particle surface occurs at $K_F^* = 10$, where there are limited events where the polymer does not adhere at least one monomer. These occurrences are likely only caused when the polymer misses the particle surface during advection. As the FENE potential strength is increased, by $K_F^* = 30$, the full-adsorption probability is reduced though increases again by $K_F^* = 50$. It has been previously shown that high FENE potential polymers with low bending rigidities will eventually undergo full adsorption provided there is vacant area surrounding the monomers as long as one monomer has adsorbed onto the surface, since the strong attractive potential causes them to sample locations very close to the initial adsorbed bead, eventually adhering to the surface. At low FENE potential strengths, the effective polymer length and radius of gyration is larger due to the monomers residing further apart from each other, hence collision with a vacancy on the surface is more likely leading to an increased adsorption rate. It seems that the midrange K_F^* lies between these two ideal conditions and so the full-adsorption probability is reduced. Furthermore, the peak at $N_A = 0$ for the two increased FENE potential strengths implies that their lower radii of gyrations leads to more occasions where the particle is missed during advection. The number of tail beads present in the final state shows less sensitivity to the FENE potential strength. We observe that the longest tails occur in the $K_F^* = 50$ simulation, whereas the $K_F^* = 10$ polymers tend to possess more tails distributed across the midrange $10 \leq N_T \leq 20$, more ideal for flocculation purposes.

Probability density functions of the total percentage of fully-adsorbed beads are presented in Fig. 10. We observe that by lowering the FENE potential strength, the adsorption rate is increased significantly, with the majority of events leading to between 40% and 60% monomer adsorption. We also see the secondary peak diminish as more events take place where polymers interact with the particle surface (i.e. they do not miss the particle due to their increased radii of gyration). Increasing K_F^* from the base case also increases the adsorption rate but only slightly.

Finally, by varying the number of initially injected polymer chains, N_P, the effect of polymer concentration on the adsorption behaviour within a shear flow may be studied. Here, we choose to increase the number of injected polymers from the base case value in order to discern the effects of steric stabilization, wherein the surface of the particle becomes saturated with monomer adsorption sites, reducing the chance
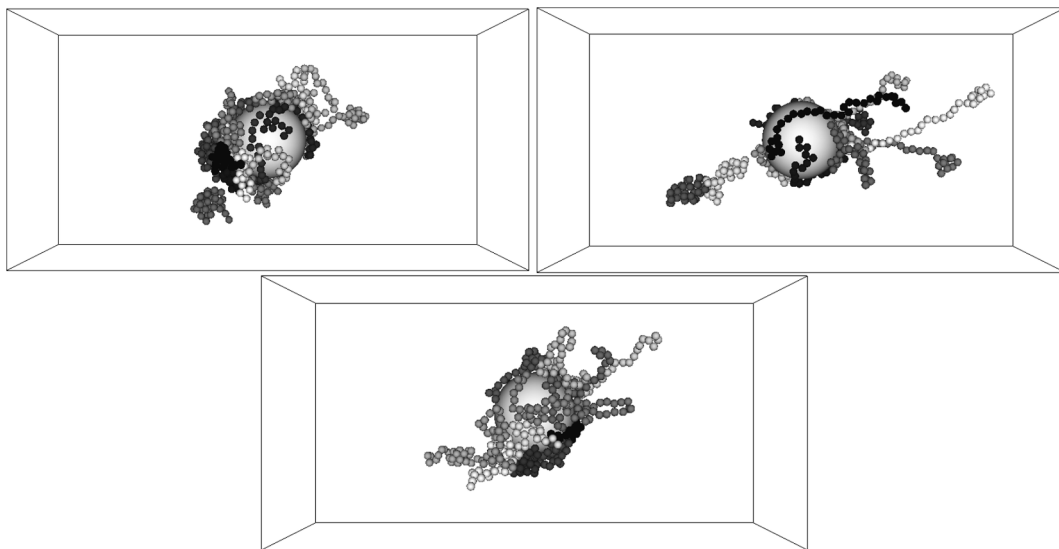

Fig. 7. Effect of bending rigidity potential strength on the probability density functions of the percentage of fully-adsorbed beads across all polymers, N_{FA}.

Fig. 8. Instantaneous snapshots of polymer-particle interaction at the final adsorbed state at $t^* = 10$. Upper-left: $K_F^* = 10$; upper-right: $K_F^* = 30$; lower: $K_F^* = 50$.
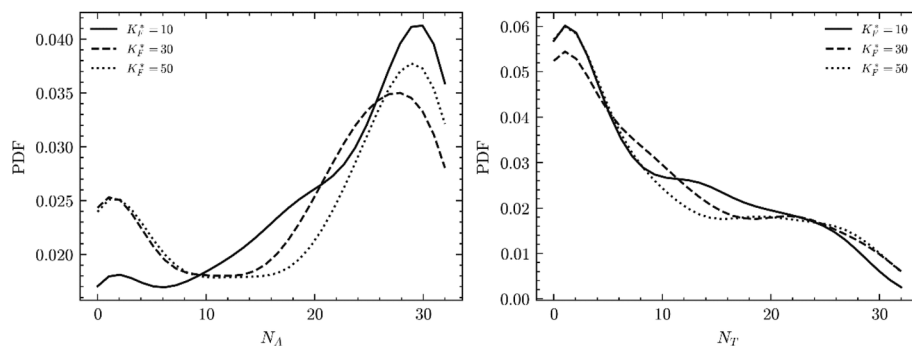

Fig. 9. Effect of FENE potential strength on the probability density functions of the number of adsorbed beads from a single polymer, N_A (left) and number of tail beads, N_T (right).
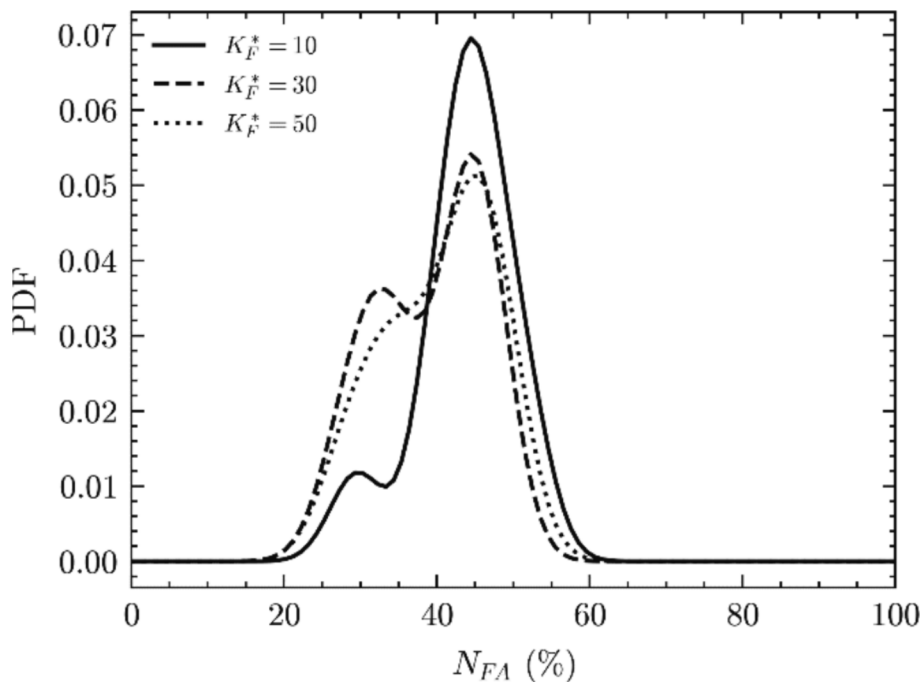

Fig. 10. Effect of FENE potential strength on the probability density functions of the percentage of fully-adsorbed beads across all polymers, N_{FA}.

or availability for further adsorption. This has consequences for further behaviours in flocculation settings, since if the surface is saturated, there is reduced potential for tails from other particle-polymer systems to interact and form bridges.

The effect of the initial polymer concentration on the eventual state of example adsorption events is illustrated in Fig. 11. Increasing the concentration from the base case to $N_P = 25$ shows an increase in the complexity of the structure formed, with tails on either side of the particle, and enhanced adsorption on the underside (lower streamwise velocity) region of the particle surface. Interestingly, it appears that some polymers which are not adsorbed onto the particle become entangled in the tails. Spreading out across the particle is still observed, and there is still vacant area on the particle for other adsorption to take place, though this is in an increased velocity region, reducing the chance of this occurring. In this case, the underside of the particle is saturated with monomers, which is not ideal for flocculation via bridging. When the concentration further increases to $N_P = 35$, the entire particle becomes saturated with polymers, and though tails are present, they are much shorter due to the compaction of nearby monomers. There is also evidence of some polymers which were unable to adsorb to the particle surface, with some likely loosely bound in the second monomer layer, not fully adsorbed to the particle.

Fig. 12 (left) shows the effect of the number of injected polymers on the monomer adsorption dynamics. As the polymer concentration increases, the number of monomers in a chain which are fully adsorbed starts to reduce, as the vacancies for new adsorption sites reduce when the surface becomes saturated. Due to steric stabilization, where the attractive potential surrounding the particle is screened by the existence of monomers, the frequency of additional adsorption events is lowered. This leads to an increase in events where only a few of the beads actually adsorb onto the surface. This is in line with Fig. 12 (right) which shows an increase in the number of tail beads for higher concentrations, though beyond $N_P = 25$, the disparity reduces slightly, indicating similar behaviour once the surface becomes saturated.

Fig. 13 shows the PDF of total percentage of fully-adsorbed beads across all polymers in each ensemble. As the concentration increases, fewer beads result in full absorption, in agreement with the previous observations and confirming that surface saturation is taking place. Furthermore, the distributions are much narrower, and by $N_P = 35$, the profile does not contain the secondary peak associated with the existence of polymers with long tails (where only a small amount of the monomers actually adsorb onto the surface). It can be ascertained that the eventual final state at high concentrations is hence made up of either collapsed polymers which fully adsorb onto the surface, or polymers which do not undergo an interaction and either miss the particle or interact for a short time, with the attraction potential not strong enough to instigate adsorption (such as in the case of a fully saturated monomer layer for instance). These findings demonstrate agreement with previous experimental studies which indicate that for increased polymer concentrations, for steritcally stabilised systems, the subsequent addition of free polymers becomes more and more energetically unfavourable as the depletion layer builds, hence fully adsorbed polymers becomes decreasingly possible (Tadros, 1991; Lockwood et al., 2023). These observations further underline the importance of polymer concentration in flocculating systems, since concentration must be mediated in order to ensure vacancies are present for subsequent bridging. That said, with sensible tuning, concentration has also been shown to promote the existence of polymer tails upon adsorption, which should be further investigated.

4. Conclusions

A novel simulation method based on particle-polymer adsorption has been developed to investigate the basic principles of flocculation and the interaction between polymers and particle surfaces. The behaviour of the polymer component was simulated using the FENE bead-spring technique and time-evolved using Langevin dynamics. The calculations considered both the non-linear and exclusion interactions within the polymer chain as well as the bending rigidity potential described by Kratky-Porod theory. The particle component was represented by a computational sphere with a finite size, and its steric interaction with the polymer beads was modelled using a modified truncated Lennard-Jones potential. Simulations of multi-polymer particle adsorption events have been performed using this technique to determine the sensitivity to two key polymer properties, the bending rigidity and the FENE non-linear spring potential.

The Kratky-Porod bending rigidity potential has proven to significantly impact the conformation of polymer chains during the process of adsorption. By examining the influence of the potential strength we have gained insights into the behaviour of polymer chains when interacting with particles. At lower rigidity values, polymers readily adhere to the particle surface, spreading out and achieving high surface coverage. However, as rigidity increases, the inability to flatten results in the formation of cluster-like conformations with elongated tails, often aligned in the streamwise direction leaving further surface for more interactions to occur. Notably, polymers with $K_B^* = 3$ exhibit the largest
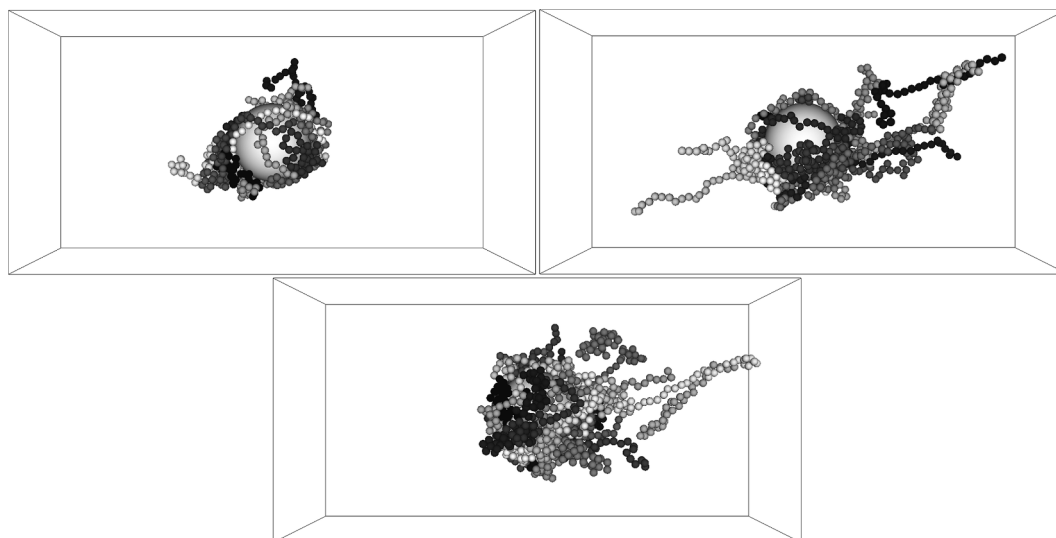

Fig. 11. Instantaneous snapshots of polymer-particle interaction at the final adsorbed state at $t^* = 10$. Upper-left: $N_P = 15$; upper-right: $N_P = 25$; lower: $N_P = 35$.
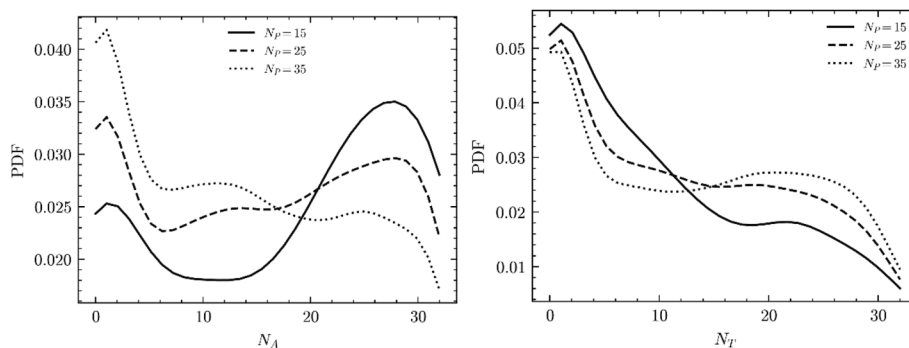
Fig. 12. Effect of number of injected polymers, N_P, on the probability density functions of the number of adsorbed beads from a single polymer, N_A (left) and number of tail beads, N_T (right).
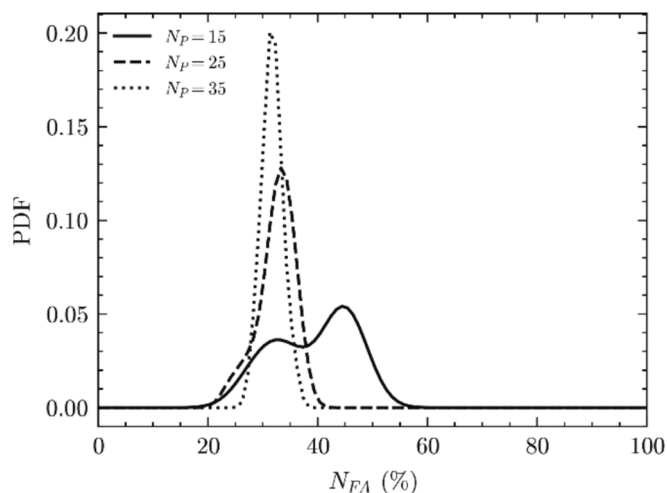

Fig. 13. Effect of number of injected polymers, N_P, on the probability density functions of the percentage of fully-adsorbed beads across all polymers, N_{FA}.

tails, with approximately one-third of their chains still present in the adsorption region. This results in an increased effective particle radius, which holds significant implications for flocculation processes. The presence of polymer loops and tails extending from the surface enhances the likelihood of bridging with other nearby particles, thereby facilitating further adsorption events. Higher bending rigidities result in a decreased likelihood of polymers missing the particle or being removed from the surface. This is attributed to the increased radii of gyration of these polymers, which enhances their collision probability with the particle due to a tendency to straighten out more compared to the curled up $K_B^* = 1.0$ polymers. None of the simulations resulted in zero monomers being adsorbed, with a minimum of 20% of the total beads adsorbing onto the particle surface in all cases. The case with $K_B^* = 1.0$ had the lowest percentage peak, with approximately 30% of the total monomers reaching the particle. Single-polymer studies indicated that these polymers spread out across the particle surface, limiting the available area for further adsorption due to their exclusion radii. With increasing bending rigidity, the modal percentage of fully adsorbed beads also increased. However, the highest adsorption percentage, around 60%, was observed at the midrange bending rigidity, $K_B^* = 3.0$. This is likely due to the higher rigidity of polymer chains, enabling them to wrap around the particle surface instead of spreading out within a localized region. Consequently, this leads to the creation of wider areas capable of absorption.

The strength of the FENE potential, K_F^*, is also a critical factor influencing adsorption dynamics. Lower K_F^* values are demonstrated to enhance adsorption efficiency, resulting in a semi-adsorbed state with

tails similar in length to the fully-adsorbed section of the polymer. This is beneficial for flocculation applications as it maintains a strong bond while increasing the effective radius of gyration. For low K_F^*, most polymers spread out across the particle surface, exhibiting tails extending in the streamwise direction in regions of increased fluid velocity. As the potential strength increases, full adsorption becomes less likely, with polymers conforming around the particle and straightening out, resulting in fewer fully adsorbed polymers. However, at $K_F^* = 50.0$, there is an increase in adsorption, accompanied by slightly larger tails compared to the $K_F^* = 10.0$ simulation. Decreasing the FENE potential strength significantly enhances the total monomer adsorption rate, with the majority of events resulting in 40% to 60% monomer adsorption. More interactions occur between polymers and the particle surface, reducing the likelihood of polymers missing the particle due to their increased radius of gyration.

The study finally demonstrates the significant impact of polymer concentration, represented by the number of initially injected polymer chains, on adsorption behaviour within a shear flow environment. Increasing polymer concentration leads to enhanced surface saturation, wherein the particle has reduced monomer adsorption sites, limiting further adsorption opportunities. This phenomenon, known as steric stabilization, reduces the likelihood of tail formation and bridging between particle-polymer systems, crucial for effective flocculation processes. Our findings illustrate that as concentration increases, the complexity of the final structure grows, with more polymers becoming entangled with others and the entire particle surface becoming saturated. The decrease in fully adsorbed beads with increasing concentration underlines the importance of managing polymer concentration to maintain optimal flocculation conditions. These insights emphasize the necessity of controlling polymer concentration in practical applications to ensure the availability of vacant sites for effective bridging and successful flocculation.

Based on the present study, the ideal conditions for flocculation involve a low to moderate concentration (based on the length and thickness of the polymers with respect to the particle surface area) of polymers, with bending rigidity of $K_B^* = 3.0$ and a low FENE potential strength $K_F^* = 10.0$ to maximize adsorption efficiency and promote the formation of tails while maintaining a strong bond between the polymer and the particle.

CRediT authorship contribution statement

L.F. Mortimer: Writing – review & editing, Writing – original draft, Visualization, Validation, Software, Methodology, Investigation, Formal analysis, Data curation, Conceptualization. **M. Fairweather:** Writing – review & editing, Supervision, Resources, Project administration, Methodology, Investigation, Funding acquisition, Conceptualization.

Declaration of competing interest

The authors declare that they have no known competing financial interests or personal relationships that could have appeared to influence the work reported in this paper.

Acknowledgements

Data availability

Data will be made available on request.

References

Brackley, C.A., 2020. Polymer compaction and bridging-induced clustering of protein-inspired patchy particles. J. Phys. Condens. Matter 32, 314002.

Buffle, J., Leppard, G.G., 1995. Characterization of aquatic colloids and macromolecules. 1. Structure and behavior of colloidal material. Environ. Sci. Technol. 29, 2169–2175.

Colby, R.H., 2010. Structure and linear viscoelasticity of flexible polymer solutions: comparison of polyelectrolyte and neutral polymer solutions. Rheologica Acta 49, 425–442.

Dickinson, E., Eriksson, L., 1991. Particle flocculation by adsorbing polymers. Adv. Colloid. Interface Sci. 34, 1–29.

Doyle, P.S., Shaqfeh, E.S., Gast, A.P., 1998. Rheology of polymer brushes: A Brownian dynamics study. Macromolecules 31, 5474–5486.

P.F. Fischer, J.W. Lottes and S.G. Kerkemeier. 2008. *Nek5000*. [Online]. [Accessed 1st September]. Available from: http://nek5000.mcs.anl.gov/.

Fu, Z., Kawaguchi, Y., 2013. A short review on drag-reduced turbulent flow of inhomogeneous polymer solutions. Adv. Mech. Eng. 5, 432949.

He, G.L., Messina, R., Löwen, H., Kiriy, A., Bocharova, V., Stamm, M., 2009. Shear-induced stretching of adsorbed polymer chains. Soft Matter 5, 3014–3017.

He, G.L., Messina, R., Löwen, H., 2010. Statistics of polymer adsorption under shear flow. J. Chem. Phys 132, 124903.

Heath, A.R., Bahri, P.A., Fawell, P.D., Farrow, J.B., 2006. Polymer flocculation of calcite: relating the aggregate size to the settling rate. AIChE J. 52, 1987–1994.

Joseph-Soly, S., Saldanha, T., Nosrati, A., Skinner, W., Addai-Mensah, J., 2019. Improved dewatering of clay rich mineral dispersions using recyclable superabsorbent polymers. Chem. Eng. Res. Des. 142, 78–86.

Khokhlov, A.R., Grosberg, A.Y., Pande, V.S., 1994. Statistical Physics of Macromolecules, Vol. 1. AIP press, New York.

Kulić, I.M., Mohrbach, H., Lobaskin, V., Thaokar, R., Schiessel, H., 2005. Apparent persistence length renormalization of bent DNA. Phys. Rev. E 72, 041905.

Lang, P.S., Obermayer, B., Frey, E., 2014. Dynamics of a semiflexible polymer or polymer ring in shear flow. Phys. Rev. E 89, 022606.

Lee, C.S., Robinson, J., Chong, M.F., 2014. A review on application of flocculants in wastewater treatment. Process Saf. Environ. Prot. 92, 489–508.

Li, C.Y., Cao, W.P., Luo, M.B., Li, H., 2016. Adsorption of polymer on an attractive nano-sized particle. Colloid Polym. Sci. 294, 1001–1009.

Li, C.Y., Luo, M.B., Li, H., Cao, W.P., 2017. Simulation study on the conformational properties of an adsorbed polymer on a nanoparticle. Colloid Polym. Sci. 295, 2251–2260.

Lockwood, A.P.G., Peakall, J., Warren, N.J., Randall, G., Barnes, M., Harbottle, D., Hunter, T.N., 2021. Structure and sedimentation characterisation of sheared Mg(OH)2 suspensions flocculated with anionic polymers. Chem. Eng. Sci. 231, 116274.

Lockwood, A.P., Rumney, J.R., Barnes, M.G., Dodds, J.M., Peakall, J., Hunter, T.N., 2023. Approximation of hindered zonal settling rates for flocculated inorganic/organic composite suspensions in inertial flow conditions. J. Water Process Eng. 51, 103459.

Mackay, M.E., Dao, T.T., Tuteja, A., Ho, D.L., Van Horn, B., Kim, H.C., Hawker, C.J., 2003. Nanoscale effects leading to non-Einstein-like decrease in viscosity. Nat. Mater. 2, 762–766.

Mortimer, L.F., Fairweather, M., 2023. Langevin dynamics prediction of the effect of shear rate on polymer-induced flocculation. Technische Mechanik 43, 73–82.

Öttinger, H.C., 2012. Stochastic processes in polymeric fluids: Tools and examples for developing simulation algorithms. Springer-Verlag.

Popov, Y.O., Tkachenko, A.V., 2005. Effects of kinks on DNA elasticity. Phys. Rev. E 71, 051905.

Sintes, T., Sumithra, K., Straube, E., 2001. Adsorption of semiflexible polymers on flat, homogeneous surfaces. Macromolecules. 34, 1352–1357.

Smith, D.E., Babcock, H.P., Chu, S., 1999. Single-polymer dynamics in steady shear flow. Science 283, 1724–1727.

Starr, F.W., Schroder, T.B., Glotzer, S.C., 2001. Effects of a nano-sized filler on the structure and dynamics of a simulated polymer melt and the relationship to ultra-thin films. Phys. Rev. E 64, 021802–021806.

Stoll, S., Buffle, J., 1996. Computer simulation of bridging flocculation processes: the role of colloid to polymer concentration ratio on aggregation kinetics. J. Colloid Interface Sci. 180, 548–563.

Tadros, T.F., 1991. Steric stabilisation and flocculation by polymers. Polym. J. 23, 683–696.

Tambo, N., 1991. Basic concepts and innovative turn of coagulation/flocculation. Wat. Supply 9, 1–10.

Tree, D.R., Muralidhar, A., Doyle, P.S., Dorfman, K.D., 2013. Is DNA a good model polymer? Macromolecules 46, 8369–8382.

Vajihinejad, V., Gumfekar, S.P., Bazoubandi, B., Najafabadi, Z.R., Soares, J.B.P., 2019. Water soluble polymer flocculants: synthesis, characterization, and performance assessment. Macromol. Mater. Eng 304, 1800526.

Vologodskii, A., Frank-Kamenetskii, M.D., 2013. Strong bending of the DNA double helix. Nucleic Acids Res. 41, 6785–6792.

White, S.I., Mutiso, R.M., Vora, P.M., Jahnke, D., Hsu, S., Kikkawa, J.M., Li, J., Fischer, J.E., Winey, K.I., 2010. Electrical percolation behavior in silver nanowire-polystyrene composites: simulation and experiment. Adv. Funct. Mater. 20, 2709–2716.

Zhou, Y., Franks, G.V., 2006. Flocculation mechanism induced by cationic polymers investigated by light scattering. Langmuir 22, 6775–6786.